J. Phys.: Condens. Matter **21** (2009) 355006 (6pp) doi:10.1088/0953-8984/21/35/355006

Phase stability of $AlYB_{14}$ sputtered thin films

Helmut Kölpin[1], Denis Music[1], Graeme Henkelman[2], Jens Emmerlich[1], Frans Munnik[3] and Jochen M Schneider[1]

[1] Materials Chemistry, RWTH Aachen University, Kopernikusstraße 16, D-52074 Aachen, Germany
[2] Department of Chemistry and Biochemistry, The University of Texas at Austin, Austin, TX 78712-0165, USA
[3] Institute of Ion Beam Physics and Materials Research, Forschungszentrum Dresden-Rossendorf, PO Box 510119, D-01314 Dresden, Germany

Received 29 May 2009, in final form 10 July 2009
Published 7 August 2009
Online at stacks.iop.org/JPhysCM/21/355006

Abstract
$AlYB_{14}$ (*Imma*) thin films were synthesized by magnetron sputtering. On the basis of x-ray diffraction, no phases other than crystalline $AlYB_{14}$ could be identified. According to electron probe microanalysis, energy dispersive x-ray analysis and elastic recoil detection analysis, the Al and Y occupancies vary in the range of 0.73–1.0 and 0.29–0.45, respectively. Density functional theory based calculations were carried out to investigate the effect of occupancy on the stability of $Al_xY_yB_{14}$ (x, $y = 0.25, 0.5, 0.75, 1$). The mean effective charge per icosahedron and the bulk moduli were also calculated. It is shown that the most stable configuration is $Al_{0.5}YB_{14}$, corresponding to a charge transfer of two electrons from the metal atoms to the boron icosahedra. Furthermore, it is found that the stability of a configuration is increased as the charge is homogeneously distributed within the icosahedra. The bulk moduli for all configurations investigated are in the range between 196 and 220 GPa, rather close to those for known hard phases such as α-Al_2O_3.

1. Introduction

Icosahedral structures, with five-fold symmetry, are rarely observed in nature. Exceptions in the field of biology are virus particles and in the field of materials, boron-rich solids [1]. Several kinds of icosahedral boron-rich solids are known, such as borane ($B_{12}H_{12}$), α-rhombohedral boron (B_{12}), icosahedral boron pnictides (e.g. $B_{12}As_2$, $B_{12}P_2$), boron suboxide (B_6O), boron carbides ($B_{1-x}C_x$) and boron-rich metal borides (XMB_{14}; X, M = usually metals) [1–5]. Two common features of these materials are outstanding hardness and high melting temperatures up to 2400 °C, making these borides useful for wear resistance applications [1, 4]. Moreover, it has been reported that radiation-induced atomic vacancies and interstitials in icosahedral borides spontaneously recombine, which is referred to as 'self-healing' behaviour [4]. Therefore, these solids possess excellent radiation resistance, allowing for application in beta voltaic devices, which convert the energy of beta-particles into electrical energy [4]. Borides often have unusual electronic and thermal properties. Boron carbides, for example, combine high electrical conductivity with high thermal resistivity, offering the potential for high temperature thermoelectric [3]. The boron-rich metal borides exhibit excellent mechanical properties as well. The mechanical properties of $AlMgB_{14}$ and $AlMgB_{14}$–TiB_2 mixtures have been investigated in detail; they possess hardness values which compete with other ultrahard materials such as cubic BN, probably the second hardest known material [6–8]. Compared with diamond and cubic BN, $AlMgB_{14}$ exhibits lower density, high chemical stability and excellent electrical conductivity which makes it useful for numerous applications, such as cutting tools, hard and erosion-resistant coatings, wear resistant electrical switch coatings and conductive thin films for microelectromechanical systems [9]. To the best of our knowledge, direct synthesis of crystalline $AlMgB_{14}$ and its XMB_{14} counterparts has not yet been achieved.

Electronic structure calculations have been carried out to investigate the diversity of properties and complex crystal structures. Boron being a light element, possesses three valence electrons, but four bonding orbitals. Therefore, boron-rich components tend to form polyhedra, such as octahedral or icosahedral units, where bonding orbitals are shared by more than two atoms (i.e. three-fold bonds) even though they contain only two electrons, as two-fold bonds do [2]. In

 © 2009 IOP Publishing Ltd Printed in the UK

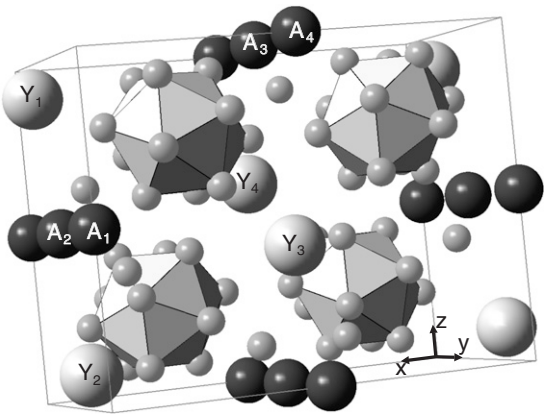

Figure 1. Unit cell of $AlYB_{14}$ structure (space group: *Imma*), where small, dark and bright spheres present B, Al and Y atoms, respectively. The positions of the metal sites are: A_1 (0; 0; 0.5), A_2 (0; 0.5; 0.5), A_3 (0.5; 0.5; 0), A_4 (0.5; 0; 0), Y_1 (0; 0.25; $1 - x$), Y_2 (0; 0.75; x), Y_3 (0.5; 0.75; $0.5 - x$), Y_4 (0.5; 0.25; $0.5 + x$); $x = 0.098\,21$.

the boron-rich boride structure the main building block is usually an icosahedron, with 12 boron atoms at the vertices [2]. As discussed by Emin *et al* [3, 4], one electron from each boron atom is bonded externally and the other two electrons participate within the internal bonding of the icosahedron. Each icosahedron has 13 orbitals which encompass the surface, including s, p, d and f orbitals. The f orbitals are located in the centres of the triangular icosahedral faces. To fill all 13 orbitals, 26 electrons are necessary (two electrons per orbital); 24 electrons are provided by the icosahedral boron atoms and two additional electrons originate from the surrounding constituents. The screening of the nuclear charge of each boron atom in an icosahedron is low, which is the reason for the high bianion affinity of an icosahedron, i.e. they exhibit a strong tendency to garner two additional electrons to form bianions like borane ($B_{12}H_{12}$).

Figure 1 shows the orthorhombic unit cell of XMB_{14} (space group *Imma*) including all four structural units. A full structural description of $AlYB_{14}$ can be found in table 1. Typically, the metal sites are not fully occupied if the metal atom possesses more than two valence electrons [2]. The boron framework of the boron-rich metal borides (XMB_{14}) consists of one icosahedral unit (B_{12}) and two isolated boron atoms. One half of the external bonds of each icosahedron are formed with adjacent icosahedra, while the other half is linked with the isolated boron atoms. All of these external bonds are two-fold bonds. These isolated boron atoms are bonded with three icosahedra and one isolated boron atom. Based on this simple orbital analysis, two electrons are required from each icosahedron and one electron from each isolated boron atom to fill all bonding orbitals, i.e. four electrons per B_{14} unit ($B_{12} + 2B$), which are supplied by the metal atoms [2].

It remains unclear, however, if valence electrons are transferred to the boron framework until all orbitals are filled, or if the metal valence electrons are only partially transferred and how the stability of the $AlMgB_{14}$ structure is thus affected.

In the case where X is Al and M is Y, where both species have three valence electrons, a bulk sample with the composition $Al_{0.71}Y_{0.62}B_{14}$ was reported [10]. Summing the valence electrons of the metals in this configuration gives a total of 3.99. Transferring all of these electrons to the boron framework and thus filling the orbitals, it is expected that such a configuration will be more stable than configurations with different valence electron populations of the metal sublattice [2]. However, Peters *et al* suggested a range of possible X and M metal site occupancies [11]. It was also shown from calculations that configurations with two different occupancies of $XMgB_{14}$ phases may be stable [5]. Hence, the relationship between charge transfer and stability for the $AlYB_{14}$ systems or the related XMB_{14} compounds remains intriguing.

Table 1. Relaxed fractional coordinates for all Wyckoff positions (x, y, z) in $AlYB_{14}$ (space group: *Imma*).

Atom	Site	x	y	z
Al	4b	0.0000	0.0000	0.5000
Y	4e	0.5000	0.2500	0.6015
B1	8i	0.1603	0.2500	0.4160
B2	8i	0.1084	0.2500	0.6224
B3	16j	0.1704	0.0016	0.2980
B4	16j	0.3108	0.0869	0.4121
B5	8i	0.0828	0.2500	0.2156

The scope of this paper is to explore the relationship between charge transfer and stability by synthesizing stable configurations of $AlYB_{14}$ in addition to the bulk sample composition $Al_{0.71}Y_{0.62}B_{14}$ [10] and to study the relationship between electronic structure and stability for different configurations of $AlYB_{14}$. Combinatorial magnetron sputtering was chosen to prepare crystalline $AlYB_{14}$ thin film samples, since a wide spread in composition and several different configurations can be obtained within a single deposition experiment. Complementary, theoretical studies investigating the stability and mean effective charge per icosahedron in $Al_xY_yB_{14}$ ($x, y = 0.25, 0.5, 0.75, 1$) were also carried out. We show that the most stable configuration is $Al_{0.5}YB_{14}$ giving an optimal charge transfer of two electrons from the metal atoms to the boron icosahedral framework.

2. Experimental methods

$Al_xY_yB_{14}$ samples were synthesized by magnetron sputtering within a combinatorial setup [12]. Targets of pure B, Y and Al were used for deposition under the following conditions: targets–substrate distance of 90 mm, RF power density of 9.2 W cm^{-2} for B and DC power density of 7.1 and 0.05 W cm^{-2} for Al and Y, respectively. The base pressure was in the order of 1×10^{-8} Torr and the working pressure during all depositions was held constant at 3×10^{-3} Torr. Polished $Al_2O_3(0001)$ single crystals were used as substrates, which were kept at a temperature of 800 °C (calibrated by a thermocouple). The deposition rate was approximately 1.26 nm min^{-1}.

The chemical composition of the deposited films was measured with electron probe microanalysis (EPMA) and energy dispersive x-ray analysis (EDX), calibrated by the

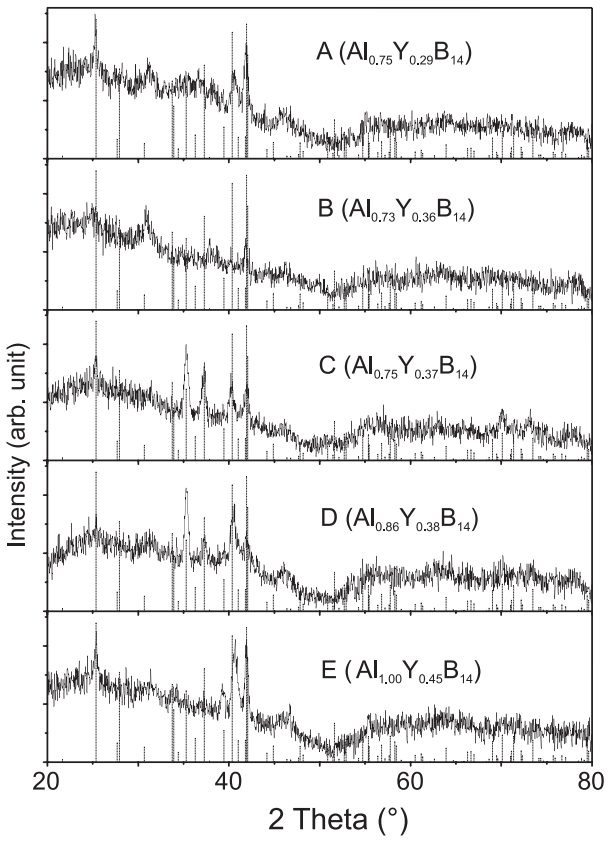

Figure 2. XRD data of the $Al_xY_yB_{14}$ ($x = 0.73$–1.00; $y = 0.29$–0.45) films. The vertical lines represent the spectrum of $Al_{0.71}Y_{0.62}B_{14}$ based on the data of Korsukova *et al* [10].

EPMA analysis. For both EPMA and EDX, a 4 kV acceleration voltage was applied. The content of light elements was determined by elastic recoil detection analysis (ERDA) with 35 MeV Cl^{7+} ions at a scattering angle of 31° [13]. Phase determination was carried out using a point-focused Bruker x-ray diffractometer equipped with a Cu Kα source operated at 40 kV and 40 mA.

3. Theoretical methods

The theoretical investigations in this work were performed using the same methodology as established in a previous work [5]. Density functional theory (DFT) [14], using the generalized-gradient approximation [15, 16] and projector augmented wave potentials [17] with Blöchl corrections for the total energy [18] were applied in all calculations. A k-point grid of $7 \times 7 \times 7$ determined by the Monkhorst–Pack scheme [19] was used to integrate over the Brillouin zone. We used a plane wave basis set with an energy cutoff of 500 eV to represent the wavefunctions. The force convergence criterion for the geometry optimization was 0.01 eV $Å^{-1}$, making sure that the ground state was reached for each configuration. These parameters were set accurate enough so that total energies were converged to within 0.01 meV. The computer program used was the Vienna *ab initio* simulation package (VASP) [17]. The internal free parameters (atomic positions) in the $Al_xY_yB_{14}$ ($x, y = 0.25, 0.5, 0.75, 1$) unit cells were relaxed first and then the lattice constants, a, b and c (orthorhombic cell), were calculated. No constrains were used for full structural relaxations carried out for each configuration. The bulk modulus was obtained by subjecting the structure to uniform compression and tension up to 6% from the equilibrium volume and fitting the energy–volume curves to the Birch–Murnaghan equation of state [20]. The energy of formation was calculated with respect to pure elemental phases, which were obtained in the same manner as described above with the following space groups: $R\bar{3}m$ for B, $P6_3/mmc$ for Y and $Fm\bar{3}m$ for Al. The $Al_xY_yB_{14}$ structure was studied in terms of effective charge, which is referred to as a difference between the charge of a neutral atom and the total charge it possesses in a compound [21]. It was calculated by Bader charge analysis [22] applying the Bader analysis program developed by Henkelman and co-workers [23, 24]. Core charges were added to the charge density distribution to verify the Bader regions [22]. The default charge density grid for one unit cell was $108 \times 60 \times 84$. To check the precision, the charge density distribution for $AlYB_{14}$ was calculated with a series of n times finer grids ($n = 2, 3, 4, 5, 6$). The deviation of the effective charge between the five and the six times finer grids was less than 0.06%. All charges of $Al_xY_yB_{14}$ ($x, y = 0.25$, 0.5, 0.75, 1) were calculated using this six times finer grid ($648 \times 360 \times 504$).

4. Results and discussion

The $Al_xY_yB_{14}$ films grown, termed here A, B, C, D and E, possess chemical compositions based on EPMA and EDX analysis of $Al_{0.75}Y_{0.29}B_{14}$, $Al_{0.73}Y_{0.36}B_{14}$, $Al_{0.75}Y_{0.37}B_{14}$, $Al_{0.86}Y_{0.38}B_{14}$ and $Al_{1.00}Y_{0.45}B_{14}$, respectively. These all differ from the chemical composition of the bulk sample $Al_{0.71}Y_{0.62}B_{14}$ [10]. The main impurities measured by ERDA in these films are less than 0.8 at.% C, 0.1 at.% H and 0.1 at.% O. These light elements may originate from residual water in the deposition chamber and carbon impurities in the B target. This hypothesis is supported by the uniform distribution of impurity elements over the film thickness, as detected by ERDA. The incorporation of H from residual water has been reported during physical vapour deposition in a high vacuum ambient before [25–27]. To the best of our knowledge, direct synthesis of crystalline $AlMgB_{14}$ films and related compounds has not been reported so far. Tian *et al* [28, 29] as well as Stock and Molin [30] have synthesized $AlMgB_{14}$ thin films, but the as-deposited state was amorphous. These samples were crystallized by annealing at 1273 K for 2 h. The XRD data of the grown films, shown in figure 2, is consistent with the previously reported bulk sample $Al_{0.71}Y_{0.62}B_{14}$ [10]. In every diffractogram the (033), (231) and (123) peaks are observed, corresponding to 2θ of 42.059°, 41.949° and 40.346°, respectively. The diffractogram of C and D contain the (220) and (132) peaks, corresponding to 2θ of 35.300° and 37.270°, while the (121) peak at 2θ of 25.374° is found in the diffractograms of A, C and E. The minor (141) peak at 2θ of 39.449° appears in the diffractogram of E. All other peaks could not be observed, especially some major peaks: (031) at

Table 2. Possible $Al_xY_yB_{14}$ (x, $y = 0.25, 0.5, 0.75, 1$) configurations including the occupied metal sites marked with a cross. The atomic positions of the metal sites are shown in figure 1. Each metal sublattice population is marked with Roman numerals.

Configuration	#	Occupied sites							
		A_1	A_2	A_3	A_4	Y_1	Y_2	Y_3	Y_4
$AlYB_{14}$	I	×	×	×	×	×	×	×	×
$Al_{0.75}YB_{14}$	I	×	×	×		×	×	×	×
$AlY_{0.75}B_{14}$	I	×	×	×	×	×	×	×	
$Al_{0.5}YB_{14}$	I	×	×			×	×	×	×
	II	×			×	×	×	×	×
	III	×		×		×	×	×	×
$Al_{0.75}Y_{0.75}B_{14}$	I	×	×	×		×	×	×	
	II	×	×	×		×		×	×
$AlY_{0.5}B_{14}$	I	×	×	×	×	×	×		
	II	×	×	×	×	×			×
	III	×	×	×	×	×		×	
$Al_{0.25}YB_{14}$	I	×				×	×	×	×
$Al_{0.5}Y_{0.75}B_{14}$	I	×	×			×	×	×	
	II	×			×	×	×	×	
	III	×		×		×	×	×	
	IV	×	×			×		×	×
	V	×			×	×		×	×
	VI	×		×		×		×	×
$Al_{0.75}Y_{0.5}B_{14}$	I	×	×	×		×	×		
	II	×		×	×	×	×		
	III	×	×	×		×			×
	IV	×		×	×	×			×
	V	×	×	×		×		×	
	VI	×		×	×	×		×	
$AlY_{0.25}B_{14}$	I	×	×	×	×	×			
$Al_{0.25}Y_{0.75}B_{14}$	I	×				×	×	×	
	II	×				×		×	×
$Al_{0.5}Y_{0.5}B_{14}$	I	×	×			×	×		
	II	×			×	×	×		
	III	×		×		×	×		
	IV	×	×			×			×
	V	×			×	×			×
	VI	×		×		×			×
	VII	×	×			×		×	
	VIII	×			×	×		×	
	IX	×		×		×		×	
$Al_{0.75}Y_{0.25}B_{14}$	I	×	×	×		×			
	II	×	×	×				×	
$Al_{0.25}Y_{0.5}B_{14}$	I	×				×	×		
	II			×		×	×		
	III	×				×			×
	IV			×		×			×
	V	×				×		×	
	VI			×		×		×	
$Al_{0.5}Y_{0.25}B_{14}$	I	×	×			×			
	II	×			×	×			
	III	×		×		×			
	IV	×	×					×	
	V	×			×			×	
	VI	×		×				×	
$Al_{0.25}Y_{0.25}B_{14}$	I	×				×			
	II	×						×	

Table 3. Calculated data of the most stable $Al_xY_yB_{14}$ configurations (x, $y = 0.25, 0.5, 0.75, 1$) including the lattice parameters (a, b and c), the mean effective charge per icosahedron ($q_{\text{eff ico}}$), the energy of formation with respect to pure elements (E_{form}) and the bulk modulus (B).

Configuration	#	a (Å)	b (Å)	c (Å)	$q_{\text{eff ico}}$	E_{form} (eV/atom)	B (GPa)
$AlYB_{14}$	I	10.504	5.912	8.271	−2.32	−0.162	219
$Al_{0.75}YB_{14}$	I	10.444	5.868	8.255	−2.13	−0.203	219
$AlY_{0.75}B_{14}$	I	10.455	5.886	8.240	−2.05	−0.162	217
$Al_{0.5}YB_{14}$	III	10.411	5.822	8.232	−2.01	−0.246	220
$Al_{0.75}Y_{0.75}B_{14}$	II	10.423	5.833	8.218	−1.85	−0.203	218
$AlY_{0.5}B_{14}$	II	10.425	5.853	8.198	−1.74	−0.161	215
$Al_{0.25}YB_{14}$	I	10.381	5.788	8.235	−1.87	−0.220	217
$Al_{0.5}Y_{0.75}B_{14}$	III	10.391	5.804	8.198	−1.71	−0.200	216
$Al_{0.75}Y_{0.5}B_{14}$	III	10.405	5.810	8.171	−1.53	−0.164	215
$AlY_{0.25}B_{14}$	I	10.397	5.838	8.154	−1.39	−0.116	213
$Al_{0.25}Y_{0.75}B_{14}$	II	10.358	5.744	8.194	−1.46	−0.151	213
$Al_{0.5}Y_{0.5}B_{14}$	IX	10.393	5.829	8.205	−1.39	−0.128	208
$Al_{0.75}Y_{0.25}B_{14}$	II	10.380	5.818	8.168	−1.18	−0.074	208
$Al_{0.25}Y_{0.5}B_{14}$	VI	10.383	5.792	8.191	−1.12	−0.072	204
$Al_{0.5}Y_{0.25}B_{14}$	V	10.366	5.807	8.175	−0.96	−0.025	203
$Al_{0.25}Y_{0.25}B_{14}$	II	10.382	5.825	8.172	−0.80	+0.037	196

2θ of 27.951° and (211) at 2θ of 33.767°. Nevertheless, all XRD peaks detected are consistent with the $AlYB_{14}$ structure. During the XRD measurements, it was observed that these samples are textured, which may explain some missing peaks in the diffractograms. Moreover, other crystalline phases in the samples are not present based on these XRD data. Hence, we present a synthesis pathway for crystalline $Al_xY_yB_{14}$ films, without an additional annealing step. The as-deposited films possess the $AlMgB_{14}$ structure but differ chemically compared to the bulk sample $Al_{0.71}Y_{0.62}B_{14}$ [10].

If the valence electrons of the metal ions in the experimentally obtained configurations A, B, C, D and E are summed up regarding the occupancies, 3.12, 3.27, 3.39, 3.78 and 4.35 electrons are delivered by the metals to stabilize the boron framework, respectively, and for the bulk sample ($Al_{0.71}Y_{0.62}B_{14}$ [10]), as previously mentioned, 3.99 electrons. Based on the orbital analysis presented above, the B framework of metal borides with the $AlMgB_{14}$ structure lacks 4 electrons in order to fill all bonding orbitals. Hence, the vapour phase condensation experiments indicate that $Al_xY_yB_{14}$ configurations other than the previously reported one [10] may be stable, even when less or more electrons are supplied by the metals.

Previous DFT based work showed that stability of these borides increases if more electrons are transferred to the boron icosahedra, but it is still not clear if the boron icosahedra require a specific number of electrons [5, 31]. To address these issues, DFT calculations were carried out in the present work, systematically investigating a wide range of different metal occupancies in the $AlYB_{14}$ system ($Al_xY_yB_{14}$ (x, y = 0.25, 0.5, 0.75, 1)) in terms of their electronic structure–stability relationship. One unit cell was employed for the calculation, limiting the possible metal sublattice populations. Table 2 summarizes all 16 possible configurations for the complete occupancy range of the $Al_xY_yB_{14}$ system. The results of the calculations are summarized in table 3: for each configuration the most stable metal sublattice population is presented, including the orthorhombic lattice parameters (a, b, c), the mean effective charge per icosahedron ($q_{\text{eff ico}}$), the

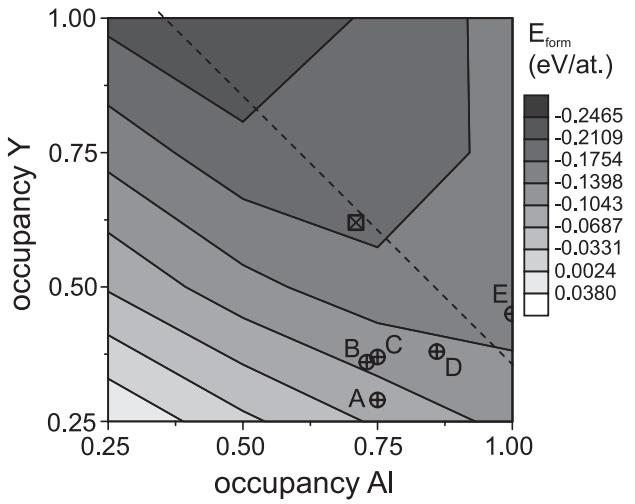

Figure 3. Energy of formation (E_{form}) as a function of the Y and Al metal site occupancy based on the calculations of $Al_xY_yB_{14}$ (x, $y = 0.25, 0.5, 0.75, 1$). The occupancies of the films (circles) and the bulk sample (square) of Korsukova *et al* [10] are provided. The dashed line represents all configurations with four valence electrons in the metal sublattice.

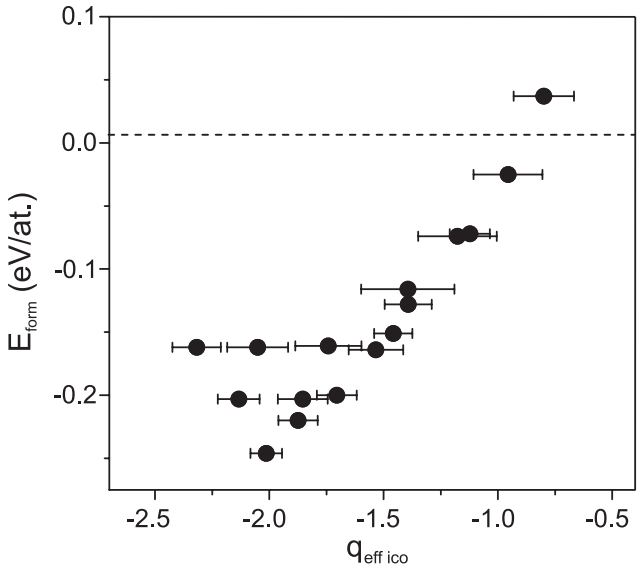

Figure 4. Energy of formation (E_{form}) as a function of the mean effective charge per icosahedron ($q_{\text{eff ico}}$) of $Al_xY_yB_{14}$ (x, $y = 0.25$, 0.5, 0.75, 1). Furthermore, the variation of the charge of the icosahedral boron atoms are presented by the horizontal bars. The dashed line separates the stable and the unstable region.

energy of formation (E_{form}) and the bulk modulus (B). It has to be noted that the most stable metal sublattice population of $Al_{0.75}Y_{0.75}B_{14}$ (here metal sublattice population number II) does not correspond to the metal sublattice population of $Al_{0.75}Mg_{0.75}B_{14}$ (metal sublattice population number I) introduced by Lee *et al* [31], which was assumed in our previous work as the basis for all studied metal borides with this composition [5]. Generally, the lattice parameters are increased with the increasing occupancy of metal sites. The lattice parameters of the bulk sample $Al_{0.71}Y_{0.62}B_{14}$ [10] are $a = 10.4310(8)$ Å, $b = 5.8212(3)$ Å and $c = 8.1947(6)$ Å. These values are in a good agreement with the calculated ones. They deviate by less than 0.3% from the lattice parameters of $Al_{0.75}Y_{0.75}B_{14}$. The bulk moduli of all configurations are in the range of 196–220 GPa, rather close to known hard phases such as α-Al_2O_3 [32]. There are no significant changes observed in the bulk modulus for the different configurations, which may indicate that the main contribution to the bulk modulus is given by the boron framework. The energy of formation is proportional to the cohesive energy and can be used to discuss the bulk modulus–stability relationship. Clearly, an increased stability of a configuration results in an increased bulk modulus. Therefore, the observed bulk modulus–stability relationship is consistent with our previous study [5].

In order to investigate the electronic structure–stability relationship of the $AlYB_{14}$ system, the energy of formation provided in table 3 is analysed in more detail. Figure 3 shows E_{form} as a function of the Y and Al metal site occupancy. Starting materials to form bulk $YAlB_{14}$ were elemental Y, Al and B [10], as in our thin film synthesis. Therefore, we calculate the energy of formation with respect to pure elemental phases. The most negative energy of formation, $E_{\text{form}} = -0.246$ eV/atom, belongs to $Al_{0.5}YB_{14}$, being the most stable configuration studied in the $Al_xY_yB_{14}$ system. It is even 64 meV/atom lower than $ScMgB_{14}$, the most stable boride configuration studied in our previous work [5]. Starting at this composition ($Al_{0.5}YB_{14}$), the energy of formation increases continuously, ending up at the unstable or metastable configuration of $Al_{0.25}Y_{0.25}B_{14}$ with a positive energy of formation. Experimentally achieved occupancies of the grown films and the bulk sample of Korsukova *et al* [10] are marked as well. Obviously, there is a large variety of different, possible configurations in this family of boron-rich compounds, which is consistent with the work of Peters *et al* [11]. Based on the calculated stability, the border between stable and unstable or metastable configurations is between configurations with a total metal site occupancy of 0.75 and 0.5. A dashed line in figure 3 indicates all configurations with four valence electrons in the metal sublattice. If all of these electrons are delivered to the boron framework, these configurations should be the most stable ones, according to the orbital analysis presented above. However, our experimental work shows they are not. Hence, there is a discrepancy between the optimal valence electron concentration in the metal sublattice, based on these two different approaches. The investigation of the mean effective charge per icosahedron supports our finding.

The mean effective charge per icosahedron data is presented in table 3. In figure 4 the energy of formation is shown as a function of the mean effective charge per icosahedron ($q_{\text{eff ico}}$) for all configurations calculated. The dashed line separates the stable ($E_{\text{form}} < 0$) and the unstable or metastable ($E_{\text{form}} > 0$) region. The mean effective charge per icosahedron varies from -2.32 to -0.80 and the most stable configuration is $Al_{0.5}YB_{14}$ where two electrons are transferred to a boron icosahedron. The phase stability generally increases if more electrons are transferred to the icosahedra, as observed in our previous work [5]. In order to discuss the charge transfer–stability relationship in more detail, we also introduce the variation of the charge of

icosahedral boron atoms as an indicator of the homogeneity of the charge distribution within the icosahedra. We suggest that icosahedra are more stable, if the transferred charge is distributed more homogeneously within the icosahedra. The most stable configuration $AlY_{0.5}B_{14}$, where two electrons are transferred to the boron icosahedra, also exhibits the most homogeneous charge distribution. Furthermore, the $AlY_{0.5}B_{14}$ configuration in fact possesses 4.5 valence electrons in the metal sublattice, while a maximum of four are expected to stabilize the boron framework according to the orbital analysis. Only two electrons are transferred to the boron icosahedra and up to two electrons may be transferred to the isolated boron atoms. Therefore, to understand the relationship between the phase stability and electronic structure of these boron-rich compounds it is insufficient to only analyse the valence electron population of the metal sublattice. It is, however, more meaningful to analyse the charge transfer to the boron framework, as carried out in this work.

5. Conclusions

$Al_xY_yB_{14}$ ($x = 0.73$–1.0; $y = 0.29$–0.45) thin films were grown by combinatorial magnetron sputtering possessing the $AlMgB_{14}$ structure. DFT calculations were carried out to study the electronic structure–stability relationship of $Al_xY_yB_{14}$ ($x, y = 0.25, 0.5, 0.75, 1$). The most stable configuration is $Al_{0.5}YB_{14}$ where two electrons are transferred to a boron icosahedron. It is shown that the stability of the $AlMgB_{14}$ structure decreases if less or more electrons are transferred to a boron icosahedron, supporting the notion that each icosahedron needs two electrons in order to fill its orbitals. Moreover, stability increases if the charge within an icosahedron is more homogeneously distributed. The calculated bulk moduli for all studied configurations lie between 196 and 220 GPa and are in agreement with the related phases [5]. It can be learnt that it is insufficient to analyse the valence electron population of the metal sublattice to understand the relationship between the phase stability and electronic structure of these boron-rich compounds. The analysis of the charge transfer to the boron framework, is therefore more meaningful.

Acknowledgments

Jochen M Schneider gratefully acknowledges funding from the Federal Ministry of Education and Research of the Federal Republic of Germany and their framework programme ‘Materials innovations for industry and society’ (Werkstoffinnovationen für Industrie und Gesellschaft—WING), represented by Projektträger Jülich, for project FKZ: 03X3507C.

References

[1] Hubert H, Devouard B, Garvie L A J, O’Keeffe M, Buseck P R, Petuskey W T and McMillan P F 1998 *Nature* **391** 22
[2] King R B 2001 *Chem. Rev.* **101** 1119
[3] Emin D 1987 *Phys. Today* **40** 55
[4] Emin D 2006 *J. Solid State Chem.* **179** 2791
[5] Kölpin H, Music D, Henkelman G and Schneider J M 2008 *Phys. Rev.* B **78** 054122
[6] Cook B A, Harringa J L, Lewis T L and Russell A M 2000 *Scr. Mater.* **42** 597
[7] Kevorkijan V, Skapin S D, Jelen M, Krnel K and Meden A 2007 *J. Eur. Ceram. Soc.* **27** 493
[8] Higashi I, Kobayashi M, Okada S, Hamano K and Lundstroem T 1993 *J. Cryst. Growth* **128** 1113
[9] Cherukuri R, Womack M, Molian P, Russel A and Tian Y 2002 *Surf. Coat. Technol.* **155** 112
[10] Korsukova M M, Lundstroem T, Tergenius L E and Gurin V N 1992 *J. Alloys Compounds* **187** 39
[11] Peters J S, Hill J M and Russell A M 2006 *Scr. Mater.* **54** 813
[12] Mertens R, Sun Z, Music D and Schneider J M 2004 *Adv. Eng. Mater.* **6** 903
[13] Kreissig U, Grigull S, Lange K, Nitzsche P and Schmidt B 1998 *Nucl. Instrum. Methods Phys. Res.* B **136–138** 674
[14] Hohenberg P and Kohn W 1964 *Phys. Rev.* **136** B864
[15] Perdew J P 1991 *Electronic Structure of Solids ‘91* ed P Ziesche and J P Eschrig (Berlin: Academic) p 11
[16] Perdew J P and Wang Y 1992 *Phys. Rev.* B **45** 13244
[17] Kresse G and Joubert D 1999 *Phys. Rev.* B **59** 1758
[18] Blochl P E 1994 *Phys. Rev.* B **50** 17953
[19] Monkhorst H J and Pack J D 1976 *Phys. Rev.* B **13** 5188
[20] Birch F 1978 *J. Geophys. Res.* **83** 1257
[21] Allred L and Rochow E G 1958 *J. Inorg. Nucl. Chem.* **5** 264
[22] Bader R 1990 *Atoms in Molecules: a Quantum Theory* (New York: Oxford University Press)
[23] Henkelman G, Arnaldsson A and Jónsson H 2006 *Comput. Mater. Sci.* **36** 354
[24] Tang W, Sanville E and Henkelman G 2009 *J. Phys.: Condens. Matter* **21** 084204
[25] Schneider J M, Anders A, Hjörvarsson B, Petrov I, Macák K, Helmersson U and Sundgren J-E 1999 *Appl. Phys. Lett.* **74** 200
[26] Schneider J M, Hjörvarsson B, Wang X and Hultman L 1999 *Appl. Phys. Lett.* **75** 3476
[27] Music D, Kölpin H, Atiser A, Kreissig U, Bobek T, Hadam B and Schneider J M 2005 *Mater. Res. Bull.* **40** 1345
[28] Tian Y, Womack M, Molian P, Lo C C H, Anderegg J W and Russell A M 2002 *Thin Solid Films* **418** 129
[29] Tian Y, Constant A, Lo C C H, Anderegg J W, Russell A M, Snyder J E and Molian P 2003 *J. Vac. Sci. Technol.* A **21** 1055
[30] Stock M and Molian P 2004 *J. Vac. Sci. Technol.* A **22** 670
[31] Lee Y and Harmon B N 2002 *J. Alloys Compounds* 338 **242**
[32] Teter D M 1998 *MRS Bull.* **23** 22